BNL-211487-2019-JAAM

Cooper Pair Density of Bi2Sr2CaCu2O8+X in Atomic scale at 4.2 K

S. H. Joo, G. Gu

To be published in "NANO LETTERS"

February 2019

Condensed Matter Physics and Materials Science Department

Brookhaven National Laboratory

U.S. Department of Energy

USDOE Office of Science (SC), Basic Energy Sciences (BES) (SC-22)

DISCLAIMER

Cooper Pair Density of $Bi_2Sr_2CaCu_2O_{8+x}$ in Atomic scale at 4.2 K

S. H. Joo[1,2], J. –J. Kim[1,2], J. H. Yoo[1,2], M. S. Park[1,2], K. S. Lee[1,2], G. Gu[3], Jinho Lee[1,2]*

[1] Department of Physics and Astronomy, Seoul National University (SNU), Seoul 08826, Republic of Korea

[2] Center for Correlated Electron Systems, Institute for Basic Science (IBS), Seoul 08826, Republic of Korea

[3]CMPMS Department, Brookhaven National Laboratory, Upton, New York 11973, USA

Abstract: In pursuit of the elusive mechanism of high-T_C superconductors (HTSC), spectroscopic imaging scanning tunneling microscopy (SI-STM) is an indispensable tool for surveying local properties of HTSC. Since a conventional STM utilizes metal tips, which allow the examination of only quasiparticles and not superconducting (SC) pairs, Josephson tunneling using STM has been demonstrated by many authors in the past. An atomically resolved scanning Josephson tunneling microscopy (SJTM), however, was realized only recently on $Bi_2Sr_2CaCu_2O_{8+x}$ (Bi-2212) below 50 mK and on the Pb(110) surface at 20 mK. Here we report the atomically resolved SJTM on $Bi_2Sr_2CaCu_2O_{8+x}$ at 4.2 K using Bi-2212 tips created *in situ*. The *I-V* characteristics show clear zero bias conductance peaks following

Ambegaokar-Baratoff (AB) theory. A gap map was produced for the first time using an atomically resolved Josephson critical current map $I_C(r)$ and AB theory. Surprisingly, we found that this new gap map is anticorrelated to the gap map produced by a conventional method relying on the coherence peaks. Quasiparticle resonance due to a single isolated zinc atom impurity was also observed by SJTM, indicating that atomically resolved SJTM was achieved at 4.2 K. Our result provides a starting point for realizing SJTM at even higher temperatures, rendering possible investigation of the existence of SC pairs in HTSC above the T_C.

Keywords: High-temperature superconductor, Josephson effect, STM

Tunneling experiments have played an important role throughout the history of superconductivity research [1-9]. Superconductor–insulator–non-superconductor (SIN) tunneling measurements, however, give information on the broken pairs, not the superconducting pairs. Fundamental difficulty of inferring superconducting properties from an SIN tunneling seems more ostensible in the case of unconventional superconductors, especially in cuprates where spectroscopic distinction between the superconducting gap and the pseudogap is subject to an ambiguity[10-12]. Conventional method - connecting the local gap values estimated from the quasiparticle coherence peaks to the superconducting pair strength - is the method of choice, while the only direct way to probe the local SC pair density is to measure the local superconducting current via Josephson tunneling. There have been many attempts to achieve this goal, for example, by utilizing Pb tips on superconductors [13, 14]. However, atomically resolved scanning Josephson tunneling microscopy (SJTM) on HTSC has been realized only recently at 50 mK or below [15, 16]. The recently reported successful atomically resolved SJTM [15] revealed the Cooper-pair density wave, which had only been theoretically hypothesized, proving the enormous potential of the SJTM technique using SC tips created *in situ*. Among the possibilities of SJTM, a temperature–dependent SJTM study on HTSC is intriguing due to the prospect of verifying the existence of local incoherent Cooper pairs above the T_C. Here, we report the first SJTM measurements at 4.2 K, which validates the possibility of SJTM above the T_C for extremely underdoped HTSC as well as at even higher temperatures.

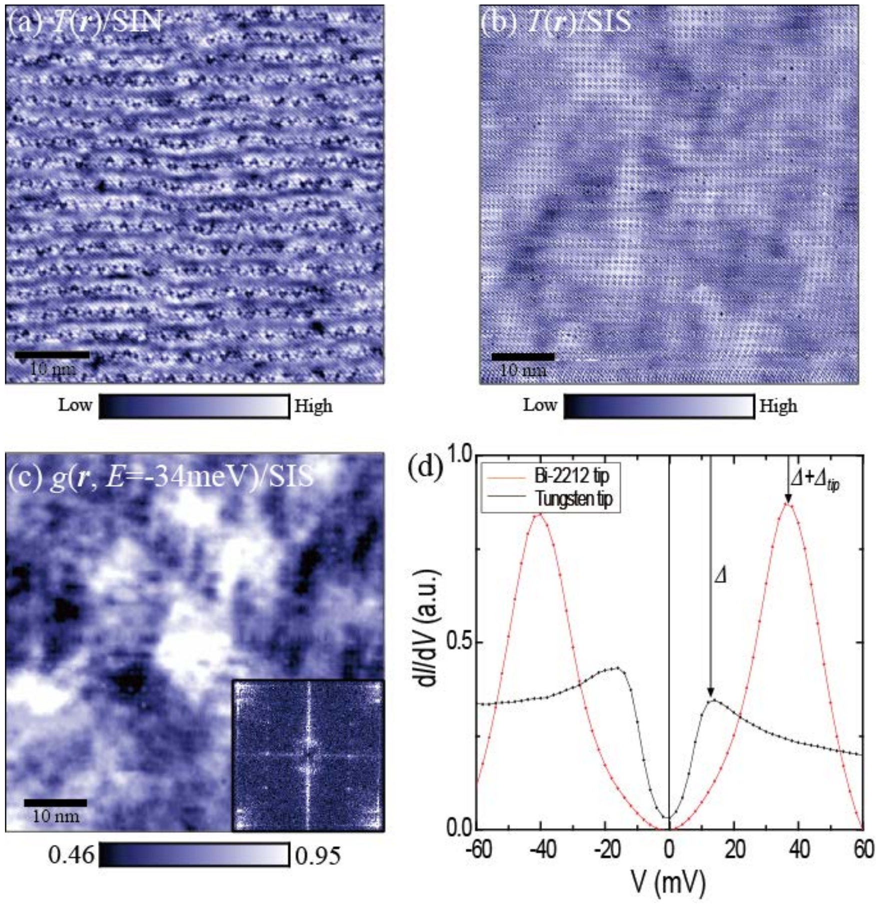

Figure 1. (a) A 50 nm × 50 nm topographic image of highly overdoped $Bi_2Sr_2CaCu_2O_{8+x}$ (Bi-2212) measured using a tungsten tip. (b) A 60 nm × 60 nm topographic image of the same sample used in (a) measured using a Bi-2212 tip. Note that the supermodulation is robust in both (a) and (b), while local properties, such as lattice vacancies, are absent in (b). (c) A 60 nm × 60 nm image of $g(\boldsymbol{r}, E = -34$ meV) using a Bi-2212 tip at the single-particle SIS junction. (Inset) Fourier transform of $g(\boldsymbol{r}, E = -34$ meV). (d) Conductance spectra measured by a tungsten tip (black curve) and a Bi-2212 tip (red curve) in the single–particle tunneling regime. As the

tip changed from a normal metal to a superconductor, the gap size changed from 14 meV to 36 meV and at the same time the amplitude of the coherence peaks become much higher. Black arrows denote the location of the coherence peaks.

For a direct measurement of the superconducting current, we performed SJTM experiments on highly overdoped Bi-2212 (T_C ~ 60 K). Floating-zone-grown single crystals of Bi-2212 were cleaved under cryogenic ultrahigh vacuum (UHV), and the cleaved samples were inserted into the STM head at 4.2 K. To obtain the SC tips *in situ*, we approached a tungsten tip to the Bi-2212 sample surface to an extremely close distance and attached a nanometer-sized small piece of Bi-2212 to the tungsten tip, forming the SC tip. Figure 1a and Figure 1b show the topographic images, measured using a tungsten tip and a Bi-2212 tip, respectively. Although we can observe supermodulation and atomic corrugation in both images, local crystalline imperfections, such as lattice vacancies, are absent in the superconductor–insulator–superconductor (SIS) topographic image (Figure 1b). This difference is due to the characteristics of the Bi-2212 tip. Because the Bi-2212 tip is not a single-atom tip like the well-prepared tungsten tip, an SIS topographic image shows an image of the convolution between the sample surface and the tip structure. Figure 1c shows a local density of states map (*LDOS* map) or $g(\boldsymbol{r}, E = -34\text{ meV})$, measured using a Bi-2212 tip forming the single-particle SIS junction. This d*I*/d*V* map and its Fourier transform (inset of Figure 1c) show that although the Bi-2212 tip is not a single-atom tip, it still retains its capability to measure local electronic structures in nanometer-resolution. Figure 1d displays a single-particle SIS junction d*I*/d*V* spectrum (red curve) as well as an SIN d*I*/d*V* spectrum (black curve) before the formation of a superconducting tip. As the tip changes from a tungsten tip to a Bi-2212 tip, the gap size changes from 14 meV to 36 meV on average, and the amplitude of coherence peaks becomes much higher (as shown by the black arrows). This verifies that we obtained a Bi-2212 tip with Δ_{tip} of about 22 meV.

As the junction resistance decreases to less than 620 kΩ, nonlinear Josephson *I-V* characteristics start to appear. Figure 2a shows the *I-V* characteristics as the junction resistance was varied from 620 kΩ to 300 kΩ. Zero bias conductance peaks can be obtained from the d*I*/d*V* curves either by numerical differentiation or direct measurement using a lock-in technique.

To analyze the Josephson tunneling features, one needs to consider the phase dynamics of the junction characterized by three energies: thermal energy, capacitive energy (E_C), and Josephson binding energy (E_J). The Josephson binding energy is given by Ambegaokar-Baratoff (AB) theory [17],

$$\boldsymbol{E_J = \frac{\hbar}{2e} I_C = \frac{\pi\hbar}{4e^2}\frac{\Delta(T)}{R_N}\tanh\left(\frac{\Delta(T)}{2k_BT}\right)} \qquad (1)$$

where $\Delta(T)$ is the superconducting gap at temperature T and R_N is the junction resistance in the normal state. (More accurately, since the equation (1) assumes that the two electrodes are identical, it needs to be modified in our case as the tip and the sample may have different order parameter amplitudes. However, we found that the correction due to the modified equation will be negligible. See supporting information section 1 for details.) For 800 kOhm resistance and Δ = 14 meV, E_J is 0.075 meV. Assuming the capacitance between the tip and the sample of about 10 fF, E_C ($2e^2/C$) amounts to 0.032 meV. [16, 18, 19] As the thermal energy k_BT is about 0.36 meV at our STM's base temperature of 4.2 K, the thermal energy dominates the phase motion. In this regime, the dynamics of the phase is diffusive. Ivanchenko *et al.* [20] and Ingold *et al.* [21] proposed the *thermally fluctuated phase diffusion* (TFPD) model for this regime which considers the thermal fluctuation due to the Johnson noise generated by a resistor Z_{env} at temperature T_n. According to this model, the *I*-*V* characteristics can be expressed as [13, 14, 20-22],

$$I(V) = \frac{I_C^2 Z_{env}}{2} \frac{V}{V^2 + V_P^2} \quad (2)$$

where $V_P = (2e/\hbar) Z_{env} k_B T_n$ and k_B is the Boltzmann constant. Since the current peak $I(V_P)$ is proportional to I_C^2, we can obtain the value directly proportional to I_C by measuring the square root of the current peak $I(V_P)$ amplitude. (see supporting information section 2.)

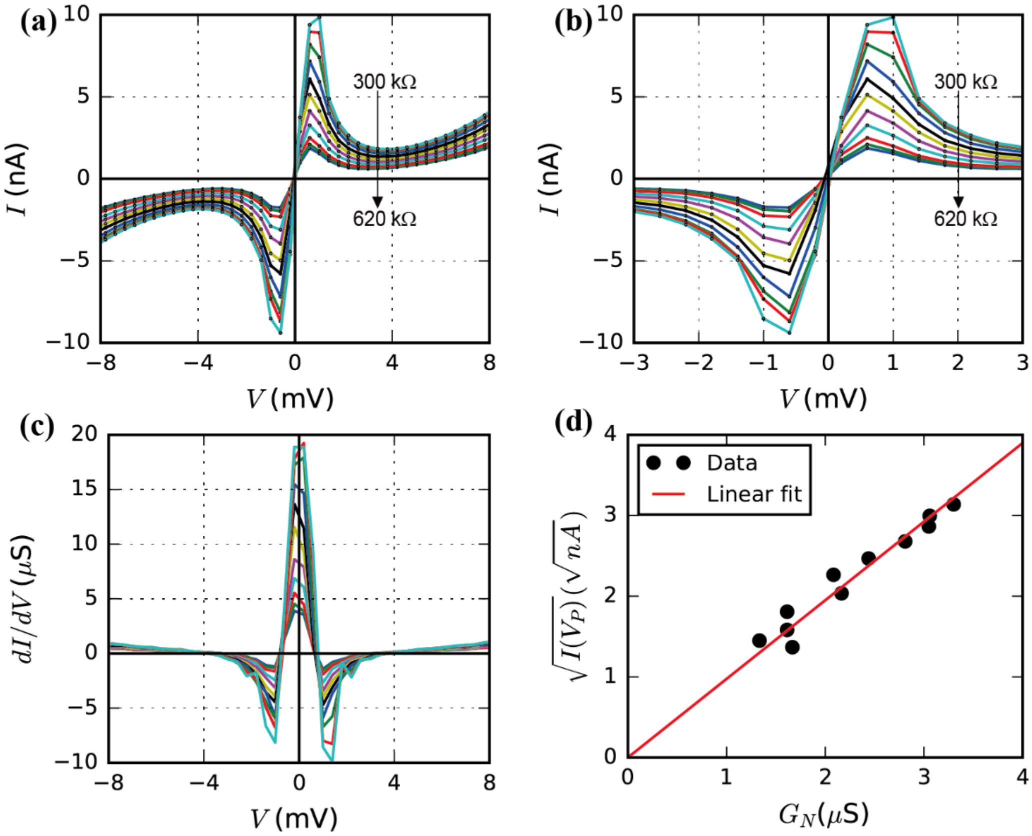

Figure 2. (a) *I*-*V* characteristics of the Josephson junction at the same location with various normal junction resistances R_N ranging from 620 kΩ to 300 kΩ at 4.2K. Zero bias conductance peaks in the d*I*/d*V* curves can be obtained either by numerical differentiation or by direct measurement using a lock-in technique. Solid circles represent the measured data while solid lines are guides for the eye. (b) Magnified *I*-*V* characteristics (a) near the zero bias voltage.

Solid circles represent the measured data while solid lines are guides for the eye. (c) d*I*/d*V* curves of (a) obtained by numerical differentiation of the curves in (a). Clear zero bias conductance peaks appear in all curves, demonstrating that the Josephson junction is successfully formed. (d) Square roots of the current peaks in (b) are plotted as black solid circles with respect to the corresponding normal conductance G_N. The red solid line shows the fit using Ambegaokar-Baratoff theory.

Figure 2b shows the magnified *I*-*V* characteristics (solid circles) in Figure 2a near the zero bias voltage. Taking the square root of the current peaks in Figure 2b gives $\sqrt{I(V_P)} \propto I_C$ and they are plotted with respect to the normal junction conductance G_N in figure 2d. The good agreement with AB theory supports that we actually achieved the Josephson junction.

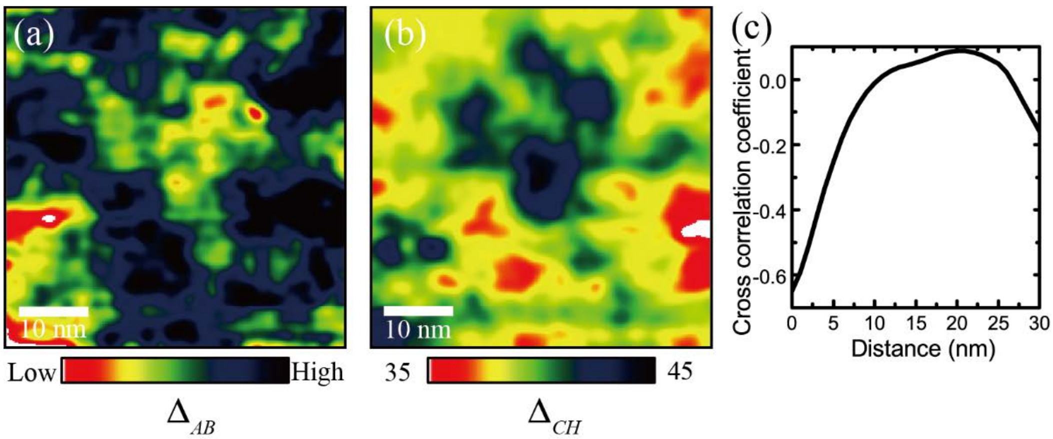

Figure 3. (a) $\Delta_{AB}(\boldsymbol{r})$, gap map produced by multiplying square root of $I(\boldsymbol{r}, V = V_P)$ and $R_N(\boldsymbol{r})$ in a 60 nm × 60 nm field of view is shown. $\Delta_{AB}(\boldsymbol{r})$ shown here is Fourier filtered. (b) Conventional gap map ($\Delta_{CH}(\boldsymbol{r})$) measured by a Bi-2212 tip in the same field of view as in (a), is shown. This gap map is obtained by locating the coherence peaks at each location with Bi-2212 tip. The

map is Fourier filtered with the same filter used in (a). (c) Azimuthally averaged cross-correlation coefficient between (a) and (b) is plotted as a function of distance. Since the cross-correlation coefficient at the center is -0.65, $\Delta_{AB}(\boldsymbol{r})$ and $\Delta_{CH}(\boldsymbol{r})$ are strongly anticorrelated.

With the SJTM capability, we measured square root of $I(\boldsymbol{r}, V = V_P)$ and multiplied it by $R_{\mathrm{N}}(\boldsymbol{r})$, which is proportional to $\Delta(\boldsymbol{r})$ according to the AB theory: $\Delta(\mathbf{r}) \propto I_C(\boldsymbol{r})R_N(\boldsymbol{r})$. (we referred to this value as $\Delta_{AB}(\boldsymbol{r})$.) Figure 3a shows $\Delta_{AB}(\boldsymbol{r})$ and Figure 3b shows a conventional gap map obtained by coherence peaks ($\Delta_{CH}(\boldsymbol{r})$) in the same field of view as Figure 3a. The anticorrelation between $\Delta_{AB}(\boldsymbol{r})$ and $\Delta_{CH}(\boldsymbol{r})$ is readily visible. To quantify the correlation between the two maps, the normalized cross-correlation between two-dimensional maps of $f(\boldsymbol{r})$ and $g(\boldsymbol{r})$ is evaluated[6],

$$C_{f,g}(\boldsymbol{R}) = \frac{\int [f(\boldsymbol{r}) - \bar{f}] \times [g(\boldsymbol{r}+\boldsymbol{R}) - \bar{g}] d^2\boldsymbol{r}}{\sqrt{A_{f,f}(0) A_{g,g}(0)}} \qquad (3)$$

where

$$A_{f,f}(\boldsymbol{R}) = \int [f(\boldsymbol{r}) - \bar{f}] \times [f(\boldsymbol{r}+\boldsymbol{R}) - \bar{f}] d^2\boldsymbol{r} \qquad (4).$$

Figure 3c shows a plot of an azimuthally averaged cross-correlation coefficient between $\Delta_{\mathrm{AB}}(\boldsymbol{r})$ and $\Delta_{CH}(\boldsymbol{r})$ vs the spatial distance r. The cross-correlation coefficient is -0.65, revealing a strong anticorrelation between the two, which is unexpected considering AB theory states $I_C R_N = \pi\Delta/2e$. The previous SJTM experiment [23] also reported a similar anticorrelation between the $I_C R_N$ product and Δ_{CH}.

This result may indicate that Δ_{AB} is more closely related to Δ_{SC}, while Δ_{CH} is related to Δ_{PG} rather than Δ_{SC}. The coexistence of two energy scales, the pseudogap and the superconducting gap, has been reported in other works [24-33]. Lawler *et al.* [34] together with Kohsaka *et al.* [35] proposed that the gap energy defined by the coherence peaks is in fact the pseudogap energy,

Δ_{PG}; meanwhile, the superconducting gap energy, Δ_{SC}, is defined by the quasiparticle interference (QPI) extinction energy [34, 35]. In addition, a magnetic-field-dependent STM study [32] reported an anticorrelation between the pseudogap and the superconducting coherence. The fact that both Δ_{AB} and Δ_{CH} as well as Δ_{SC} and Δ_{PG} have an anticorrelation suggests that Δ_{AB} is possibly related to Δ_{SC}. However, the exact relation between Δ_{SC} and Δ_{PG} or Δ_{CH} and Δ_{AB} has not been reported. Since these relations are essential to clarify the relation between Δ_{SC} and Δ_{AB}, further study, such as investigations of Δ_{AB} and Δ_{CH} over a wide range of doping, is necessary. In addition, as AB theory in d-wave superconductors is not fully established, AB theory used here may need to be corrected.

We also performed SJTM experiments on nearly optimally doped Bi-2212 for comparison. The conductance map at -1.6 mV in Figure 4a shows near zero bias peaks (NZBP), as guided by a red circle, which are not observed in other areas. These NZBPs correspond to the sharp peak below the Fermi level at the Zn impurity site, which is evident by comparing Figure 4d (red curve, marked by (i)) and the result of Pan *et al.* [36]. Since 1) the topographic image shows no sign of surface defects, while the conductance map clearly shows them, and 2) the observed NZBPs occur at -1.6 mV as in Pan *et al.*'s report [36], our data suggests that our NZBPs are due to the quasiparticle scattering resonance at the Zn impurities. (see supporting information section 5).

One intriguing feature of the spectrum near the Zn impurity is an additional peak on the empty side at +1.6 mV of the dI/dV spectrum (red curve in Figure 4d, marked by (ii)), while SIN tunneling [36] shows the

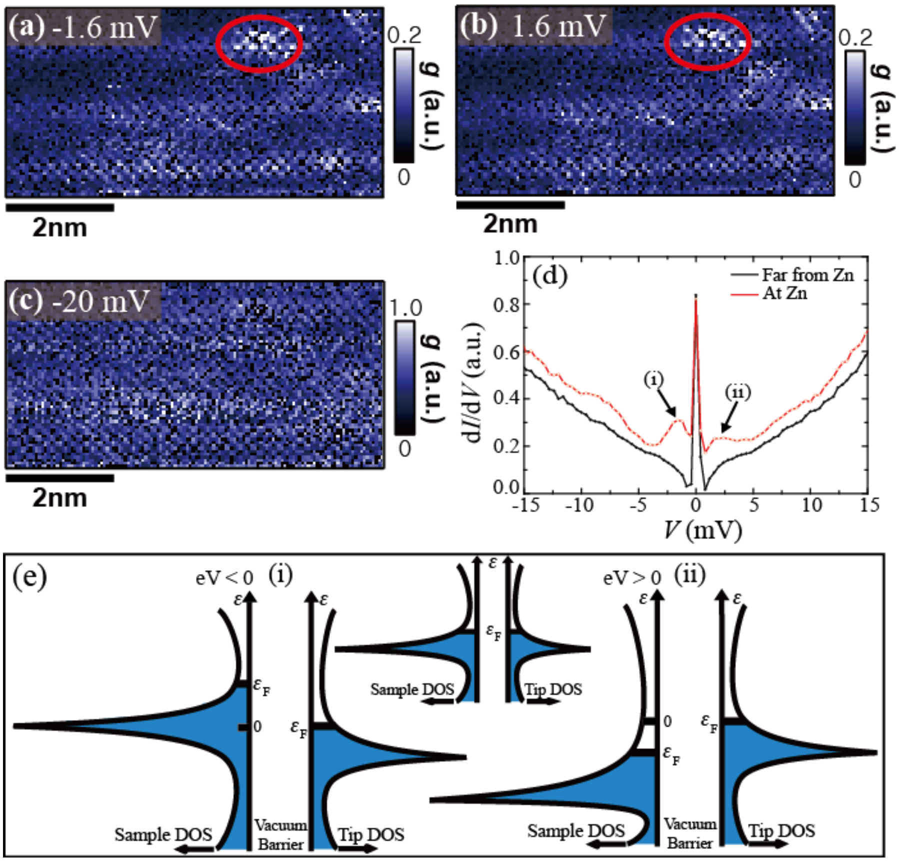

Figure 4. (a-c) Conductance map measured by a newly produced $Bi_2Sr_2CaCu_2O_{8+x}$ tip at (a) -1.6 mV, (b) 1.6 mV and (c) -20 mV. Identical unusual bright spots guided by the red circle are only observed in (a) and (b). Note that the region of these bright spots is indistinguishable in the high voltage map shown in (c). (d) The conductance spectrum of the bright spot in (a) and (b) is shown as red open circles. In addition to the zero bias conductance peak, two additional peaks, marked by black arrows, appear at both -1.6 mV and 1.6 mV. The conductance spectrum of a point far from the bright site is also presented as black filled circles for a comparison. (e) The density of states (DOS) at a Zn impurity site on the sample and the DOS of a Bi-2212 tip is drawn schematically based on the result of Pan *et al.* [36]. The Zn impurity on the sample induces a weak resonance peak on the DOS of a Bi-2212 tip due to the extremely close tip-sample distance. When there is no applied bias voltage, no tunneling current flows (inset in the

middle). Meanwhile, negative bias voltage on the sample (left figure) elevates the sample Fermi energy and when the peak in the sample DOS meets the tip's Fermi energy, the d*I*/d*V* peak appears in the negative bias voltage region (peak (i) in (d)). Positive bias voltage on the sample (right figure) lowers the sample's Fermi energy and when the peak in the tip's DOS coincides with the sample's Fermi energy, the d*I*/d*V* peak appears in the positive bias voltage region (peak (ii) in (d)).

quasiparticle scattering resonance only on the filled side. In addition, the quasiparticle scattering resonance peak height is smaller than that in the SIN case [36]. The amplitude of our impurity resonance peaks is smaller than that measured in the SIN case because both the SC tip and SC sample have extremely small density of states (DOS) near E_F (Figure 4e). We propose a simple model to describe the particle-hole symmetric resonance peaks at ±1.6 mV. To obtain the Josephson current at 4.2 K, we placed the SC tip extremely close to the Bi-2212 surface. This extremely small tip-sample distance may enable a Zn impurity on the sample to induce a resonant bound state not only on the sample but also on the Bi-2212 tip. Figure 4e shows a cartoon model explaining the particle-hole symmetric Zn resonance peaks in such a scenario. A negative bias voltage on the sample elevates the sample's Fermi energy, and when the peak in the sample's DOS coincides with the tip's Fermi energy, the d*I*/d*V* peak appears in the negative bias voltage region (peak (i) in Figure 4d). A positive bias voltage on the sample lowers the sample's Fermi energy, and when the peak in the tip's DOS induced by a Zn impurity on the sample coincides with the sample's Fermi energy, the d*I*/d*V* peak appears in the positive bias voltage region (peak (ii) in Figure 4d). (See supporting information section 6 for the SIN case for comparison). Therefore, the resonance peak at +1.6 mV is likely to be a consequence of the resonant bound state at the tip induced by a Zn impurity on the sample.

In conclusion, we demonstrated an atomically resolved SJTM with a Bi-2212 tip on a Bi-2212 sample at 4.2 K, which is the highest temperature to our knowledge at which SJTM has been realized. The topographic image and the SIS d*I*/d*V* spectrum verified that we obtained a Bi-2212 tip. All the spectra clearly show thermally fluctuated Josephson effect features and the distance-dependent Josephson zero bias conductance peaks agree with the linearity of an $I_C R_N$ product predicted by AB theory. The gap map produced using AB theory and the I_C map is anticorrelated to the gap map produced by the conventional method using coherence peaks. This may suggest that the superconducting gap defined by coherence peaks cannot simply be assumed to be related to the superconductivity alone.

Although quasiparticle tunneling experiments contributed a lot in the HTSC studies, these experiments can only study SC pairs indirectly. The absence of a theory like the BCS theory for HTSC's and the existence of pseudogap further complicates connecting single particle tunneling to SC pair density. SJTM experiment, however, can directly probe the local pair density and one can avoid such complications.

We also observed particle-hole symmetric Zn resonance peaks by SJTM, which can be explained by the Zn resonant bound states on the SC tip induced by a Zn impurity on the sample. This observation suggests the possibility of manipulating the electronic structure of the SC tip when used on another kinds of samples, as well as the possibility of realizing the proximity effect where our superconducting tip might induce a pairing potential on the normal samples when the distance between the SC tip and the sample is reduced enough.

Moreover, as we present in this report, SJTM experiment on HTSC can be successfully conducted not only at mK range but also at 4.2 K. This extended temperature range of the

SJTM suggests one extremely interesting experiment on pseudogap phase. Although many experimental and theoretical studies were devoted to elucidating this mysterious state, the origin and its relevance to SC are still controversial. Quite a few results suggest the existence of incoherent local pairs in the pseudogap phase above the T_C [37-39]. If these incoherent superconducting pair states exist at the pseudogap state as proposed [37-39], direct observation of such SC pairs in pseudogap would be a breakthrough in the understanding of the pseudogap state. Our results suggest that SJTM at 4.2 K and potentially even at a higher temperature is possible. This motivates SJTM experiments on extremely underdoped cuprates with very low T_C to directly examine the existence of incoherent pairs in pseudogap phases.

ASSOCIATED CONTENT

Supporting Information

(1) Ambegaokar-Baratoff formula. (2) Thermally fluctuated phase diffusion model. (3) $R_N(\boldsymbol{r})$ (4) Applying Ambegaokar-Baratoff theory on d-wave superconductor. (5) Topographic image and $g(\boldsymbol{r}, E)$ around Zn impurity. (6) Density of states of a $Bi_2Sr_2CaCu_2O_{8+x}$ sample at a Zinc impurity site and a tungsten tip.

AUTHOR INFORMATION

Corresponding Author

*E-mail: jinholee@snu.ac.kr

Notes

The authors declare no competing financial interest.

ACKNOWLEDGMENT

We thank the following people for discussions and communications: K. McElroy, C. Lupien, T. Hanaguri, T. W. Noh, J. -G Park, Y. Bang, G. Aeppli, S. Uchida, Y. D. Park, Y. Kuk, I. Lee, C. K. Kim and J. C. Seamus Davis. This work was supported by the Institute for Basic Science in Korea (Grant No. IBS-R009-G2) and Research Resettlement Fund for the new faculty of Seoul National University. This work was also supported by the National Research Foundation of Korea(NRF) grant funded by the Kor ea government(MSIP) (No. 2017R1A2B3009576) and the Institute of Applied Physics of Seoul National University.

Reference

1. Giaever, I.; Megerle, K. *Phys. Rev.* **1961,** 122, (4), 1101-1111.
2. Rowell, J. M.; McMillan, W. L. *Phys. Rev. Lett.* **1966,** 16, (11), 453-456.
3. Howald, C.; Eisaki, H.; Kaneko, N.; Greven, M.; Kapitulnik, A. *Phys. Rev. B* **2003,** 67, (1), 014533.
4. da Silva Neto, E. H.; Aynajian, P.; Frano, A.; Comin, R.; Schierle, E.; Weschke, E.; Gyenis, A.; Wen, J.; Schneeloch, J.; Xu, Z.; Ono, S.; Gu, G. D.; Le Tacon, M.; Yazdani, A. *Science* **2014,** 343, (6169), 393-396.
5. Zeljkovic, I.; Xu, Z.; Wen, J.; Gu, G. D.; Markiewicz, R. S.; Hoffman, J. E. *Science* **2012,** 337, (6092), 320-323.
6. McElroy, K.; Lee, J.; Slezak, J. A.; Lee, D. H.; Eisaki, H.; Uchida, S.; Davis, J. C. *Science* **2005,** 309, (5737), 1048-1052.
7. Chuang, T. M.; Allan, M. P.; Lee, J.; Xie, Y.; Ni, N.; Bud'ko, S. L.; Boebinger, G. S.; Canfield, P. C.; Davis, J. C. *Science* **2010,** 327, (5962), 181-184.

8. Fujita, K.; Kim, C. K.; Lee, I.; Lee, J.; Hamidian, M. H.; Firmo, I. A.; Mukhopadhyay, S.; Eisaki, H.; Uchida, S.; Lawler, M. J.; Kim, E. A.; Davis, J. C. *Science* **2014,** 344, (6184), 612-616.

9. Fischer, Ø.; Kugler, M.; Maggio-Aprile, I.; Berthod, C.; Renner, C. *Rev. Mod. Phys.* **2007,** 79, (1), 353-419.

10. Boyer, M. C.; Wise, W. D.; Chatterjee, K.; Yi, M.; Kondo, T.; Takeuchi, T.; Ikuta, H.; Hudson, E. W. *Nat. Phys.* **2007,** 3, (11), 802-806.

11. Zhong, Y.; Wang, Y.; Han, S.; Lv, Y. F.; Wang, W. L.; Zhang, D.; Ding, H.; Zhang, Y. M.; Wang, L. L.; He, K.; Zhong, R. D.; Schneeloch, J. A.; Gu, G. D.; Song, C. L.; Ma, X. C.; Xue, Q. K. *Sci Bull* **2016,** 61, (16), 1239-1247.

12. Misra, S.; Oh, S.; Hornbaker, D. J.; DiLuccio, T.; Eckstein, J. N.; Yazdani, A. *Phys. Rev. Lett.* **2002,** 89, (8), 087002.

13. Naaman, O.; Teizer, W.; Dynes, R. C. *Phys. Rev. Lett.* **2001,** 87, (9), 097004.

14. Kimura, H.; Barber, R. P.; Ono, S.; Ando, Y.; Dynes, R. C. *Phys. Rev. Lett.* **2008,** 101, (3), 037002.

15. Hamidian, M. H.; Edkins, S. D.; Joo, S. H.; Kostin, A.; Eisaki, H.; Uchida, S.; Lawler, M. J.; Kim, E. A.; Mackenzie, A. P.; Fujita, K.; Lee, J.; Davis, J. C. S. *Nature* **2016,** 532, (7599), 343-347.

16. Randeria, M. T.; Feldman, B. E.; Drozdov, I. K.; Yazdani, A. *Phys. Rev. B* **2016,** 93, (16), 161115.

17. Ambegaokar, V.; Baratoff, A. *Phys. Rev. Lett.* **1963,** 10, 486-9.

18. Ast, C. R.; Jack, B.; Senkpiel, J.; Eltschka, M.; Etzkorn, M.; Ankerhold, J.; Kern, K. *Nature Communications* **2016,** 7.

19. Jack, B.; Eltschka, M.; Assig, M.; Etzkorn, M.; Ast, C. R.; Kern, K. *Phys. Rev. B* **2016,** 93, (2).

20. Ivanchenko, Y. M.; Zil'Berman, L. A. *Sov. Phys. JETP* **1969,** 28, (6), 1272-1276.

21. Ingold, G.-L.; Grabert, H.; Eberhardt, U. *Phys. Rev. B* **1994,** 50, (1), 395.

22. Caldeira, A. O.; Leggett, A. J. *Physica A: Statistical Mechanics and its Applications* **1983,** 121, (3), 587-616.

23. Kimura, H.; Barber, R. P.; Ono, S.; Ando, Y.; Dynes, R. C. *Phys. Rev. B* **2009,** 80, (14), 144506.

24. Hüfner, S.; Hossain, M. A.; Damascelli, A.; Sawatzky, G. A. *Rep. Prog. Phys.* **2008,** 71, (6), 062501.

25. Kordyuk, A. A. *Low Temp. Phys.* **2015,** 41, (5), 319-341.

26. Deutscher, G. *Nature* **1999,** 397, (6718), 410-412.

27. Lee, W. S.; Vishik, I. M.; Tanaka, K.; Lu, D. H.; Sasagawa, T.; Nagaosa, N.; Devereaux, T. P.; Hussain, Z.; Shen, Z. X. *Nature* **2007,** 450, (7166), 81-84.

28. Rullier-Albenque, F.; Alloul, H.; Rikken, G. *Phys. Rev. B* **2011,** 84, (1), 014522.

29. Yoshida, T.; Malaeb, W.; Ideta, S.; Lu, D. H.; Moor, R. G.; Shen, Z. X.; Okawa, M.; Kiss, T.; Ishizaka, K.; Shin, S.; Komiya, S.; Ando, Y.; Eisaki, H.; Uchida, S.; Fujimori, A. *Phys. Rev. B* **2016,** 93, (1), 014513.

30. Kondo, T.; Takeuchi, T.; Kaminski, A.; Tsuda, S.; Shin, S. *Phys. Rev. Lett.* **2007,** 98, (26), 267004.

31. Ma, J. H.; Pan, Z. H.; Niestemski, F. C.; Neupane, M.; Xu, Y. M.; Richard, P.; Nakayama, K.; Sato, T.; Takahashi, T.; Luo, H. Q.; Fang, L.; Wen, H. H.; Wang, Z.; Ding, H.; Madhavan, V. *Phys. Rev. Lett.* **2008,** 101, (20), 207002.

32. He, Y.; Yin, Y.; Zech, M.; Soumyanarayanan, A.; Yee, M. M.; Williams, T.; Boyer, M. C.; Chatterjee, K.; Wise, W. D.; Zeljkovic, I.; Kondo, T.; Takeuchi, T.; Ikuta, H.; Mistark, P.; Markiewicz, R. S.; Bansil, A.; Sachdev, S.; Hudson, E. W.; Hoffman, J. E. *Science* **2014,** 344, (6184), 608.

33. Tanaka, K.; Lee, W. S.; Lu, D. H.; Fujimori, A.; Fujii, T.; Risdiana; Terasaki, I.; Scalapino, D. J.; Devereaux, T. P.; Hussain, Z.; Shen, Z. X. *Science* **2006,** 314, (5807), 1910.

34. Lawler, M. J.; Fujita, K.; Lee, J.; Schmidt, A. R.; Kohsaka, Y.; Kim, C. K.; Eisaki, H.; Uchida, S.; Davis, J. C.; Sethna, J. P.; Kim, E.-A. *Nature* **2010,** 466, (7304), 347-351.

35. Kohsaka, Y.; Taylor, C.; Wahl, P.; Schmidt, A.; Lee, J.; Fujita, K.; Alldredge, J. W.; McElroy, K.; Lee, J.; Eisaki, H.; Uchida, S.; Lee, D. H.; Davis, J. C. *Nature* **2008,** 454, (7208), 1072-1078.

36. Pan, S.; Hudson, E.; Lang, K.; Eisaki, H.; Uchida, S.; Davis, J. *Nature* **2000,** 403, (6771), 746-750.

37. Wang, Y.; Li, L.; Naughton, M. J.; Gu, G. D.; Uchida, S.; Ong, N. P. *Phys. Rev. Lett.* **2005,** 95, (24), 247002.

38. Wang, Y.; Li, L.; Ong, N. P. *Phys. Rev. B* **2006,** 73, (2), 024510.

39. Li, L.; Wang, Y.; Komiya, S.; Ono, S.; Ando, Y.; Gu, G. D.; Ong, N. P. *Phys. Rev. B* **2010,** 81, (5), 054510.